JME

Journal of Mining & Environment,
Vol. 9, No. 3, 2018, 727-740.
DOI: 10.22044/jme.2018.7084.1551

A three dimensional geometrical model for calculation of induced stresses surrounding longwall working

H. Mohammadi[1*] and H. Darbani[2]

1. Mining Engineering Department, Faculty of Engineering, Vali-e-Asr University of Rafsanjan, Rafsanjan, Iran
2. Tabas Negin Coal Co., Tabas, Iran

Received 16 May 2018; received in revised form 29 May 2018; accepted 2 June 2018
**Corresponding author: hamid.mohammadi@vru.ac.ir (H. Mohammadi).*

Abstract
There are various criteria that need to be examined alongside each other when designing a longwall mining system. Challenges such as determination of the supported roof width, support system design, caving height determination, lateral or chain pillar size determination, and optimum support design for the main gate and tail gate roadways have to be tackled for this aim. Three-dimensional analysis would deliver the highest accuracy of induced stresses around the longwall working area. Thus, the main purpose of this paper is to develop a three dimensional geometrical computing model (3GCM) for calculating the induced stresses in both longitudinal and transverse loading orientations of the extraction panel. 3GCM is capable of studying the changes of induced stresses along the longitudinal orientation of working and the lateral pillar as well as the induced stresses ahead and behind of the face. The proposed computational model, for analyzing the vertical induced stresses, was used in one of the longwall workings in the Parvade-2 coal mine of Tabas, Iran. Validation of 3GCM has approved its high efficiency for the analysis of induced stresses within the working as well as surrounding areas.

Keywords: *3GCM, Longwall, Induced Stress, Coal Mining.*

1. Introduction

The study of the induced stress fields surrounding longwall workings has always been one of the most interesting subjects for designers, miners, and researchers. Knowing the conditions of the induced stress fields ahead and behind of the face, it is possible to perform an optimal design of a mining system considering various aspects such as: determination of the working length (taking into account the other influential factors), study of the advance rate effect on the stress fields and determination of the optimum advance rate, design of the support system of working, and determination of the roof support width and the caving stage. In longwall method, due to the caving process, the induced stress fields surrounding working are considered as a secondary loading for the gate roadways. In other words, if the gate roadways are subjected to secondary loading during the extraction operation, most likely due to changes of the characteristics and the behavior of the excavation damaged zone (EDZ), the designed support system for the fate roadway (based on the primary characteristics of EDZ) may not present a proper performance putting the production rate of an underground mine in fatal danger. This illustrates the importance of the safety regulations and dependency of the production rate on the safety conditions of the underground opening networks [1-3].

According to the previous studies [1-3], considering the stress redistribution ahead, behind, and in sides of the face, the most accurate stress analysis within longwall working as well as its surrounding area may be delivered by a three dimensional (3D) analysis (Figure 1). Hence, almost all studies in this regard have been based on numerical modeling. However, the numerical

methods, in addition to the need for a qualified specialist, are costly and time-consuming processes, and are mostly site-dependent. In return, the analytical methods for design of rock mechanics and mining projects, despite the implementation of a simplification series to the solution process, have provided conditions that the designer or the expert, based on a set of mathematical relations, may obtain the required results at the very least possible time. In addition, analytical models have applicability to be used in a wide range of sites. Therefore, despite the many improvements in the computational processing methods for reducing the numerical modeling time, development of the analytical solutions and their application in the industry is still on the rise [4-8].

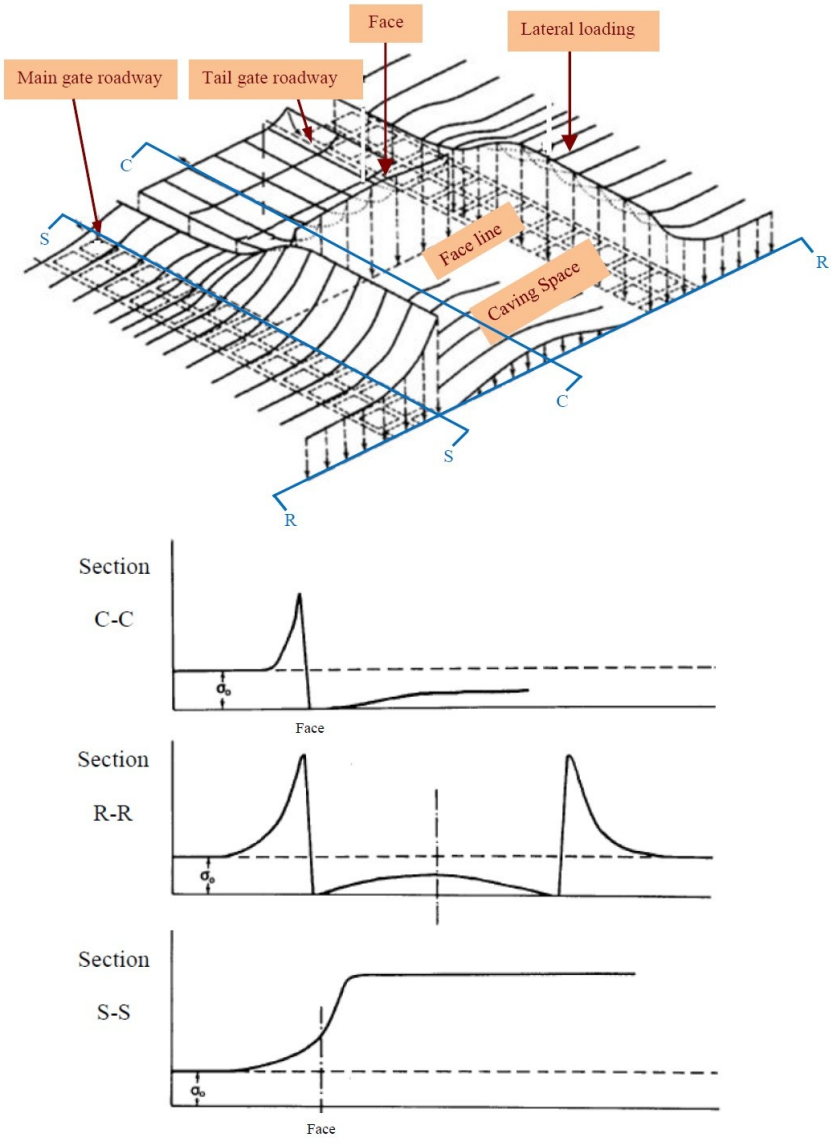

Figure 1. 3D conditions of induced stresses surrounding longwall working [3].

A review of the recent studies shows that almost no comprehensive analytical method has been presented for the 3D study of induced stress fields surrounding longwall working, and even two dimensional (2D) analytical methods to calculate the caving effect on the gate roadway stability (in the face behind) are very scarce. Therefore, the main purpose of this paper is to develop a 3D analytical model for analyzing the induced stresses surrounding longwall working. In the previous researches by the authors of this paper, a 2D geometrical computing model (GCM) to analyze the effect of secondary loading due to the caving operation on the stability conditions of gate roadways was presented [8, 9]. Therefore, in order to achieve the goal of this paper, the 2D form of GCM will be developed in 3D in such a way as to be able to calculate the conditions of

stress fields in the ahead, behind, and both sides of face. Based on this, firstly, the 2D form of GCM is discussed, and then the development process of the 3D form of GCM is presented.

2. 2D form of GCM

GCM is a computational geometry model for calculating the effect of longwall working on the main gate and tail gate roadways without any limitation to use in non-mechanized and mechanized working as well as in the cross-sectional form of gate roadways, and thus it can be considered as a comprehensive model. Figure 2 shows a schematic view of longwall working prepared for extraction operations. According to this figure, before coal mining, an EDZ has been created around the main gate and tail gate roadways. In this figure, H_i is the gate roadway depth as measured from the ground level, B_{Gi} is the gate roadway width, h_i is the gate roadway height, B_{ni} is the EDZ height, a_i is half of the EDZ width, α is the coal seam dip angle, and φ_p is the peak internal friction angle of rock mass. Subscript i defines gate roadways, i.e. i = 1 is for the main gate roadway and i = 2 represents the tail gate roadway [8, 9].

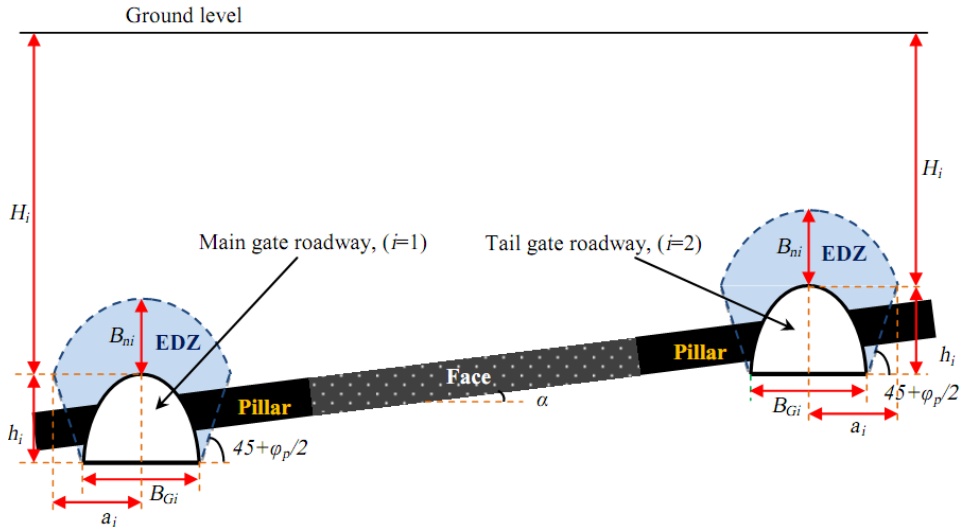

Figure 2. A schematic view of longwall working before coal extraction [8, 9].

In order to calculate the EDZ size and its displacements at the gate roadway crown (before mining operation), the following relations are used.

$$u_i = 0.1B_{Gi}\left(e^{\frac{\sigma_{0i}-\gamma q_i}{\sigma_{cm}}}-1\right) \quad (1)$$

$$B_{ni} = 2.08B_{Gi}\left(e^{\frac{\sigma_{0i}}{\sigma_{cm}}}-1\right)^{0.6} \quad (2)$$

where, u_i is the roof displacement of gate roadway (m), σ_{cm} is the compressive strength of materials above the gate roadway (MPa), q_i is the bearing capacity of the support system at the gate roadway (kPa), σ_{0i} is the vertical in situ stress at the gate roadway roof (MPa), and γ is the unit weight of the rock mass (MN/m^3).

Due to advancing coal face, a CZ above the longwall face is created and stress field is redistributed; consequently, a triangular damaged zone is created above the gate roadway and an additional loading is applied to coal pillars and EDZ, which causes an extension in EDZ [10, 11]. To calculate the face effect on EDZ of the gate roadways, GCM is presented as in Figure 3. As shown in this model, contrary to the previous models, four important subjects are considered, as follow: 1) coal seam dip, 2) vertical distance between coal pillar and the roof of gate roadway (it determines the coal seam location at sidewall of the gate roadway), 3) stability condition of tail gate roadway, and 4) different gate roadway cross-sections. According to GCM, the damaged zone is the triangle $A_iB_iC_i$, and the additional loading relates to the part of triangle $A_iB_iC_i$ located outside the parabolic area of EDZ. In Figure 3, h_s is the coal seam thickness or face height, φ_{0i} is the caving angle, β_i is the influence angle of caving zone (CZ), W_i is the pillar width, J_i is the vertical distance between the pillar and roof of gate roadway, L is the face length, and $h_{\Delta i}$ is the height of triangle $A_iB_iC_i$ [8, 9].

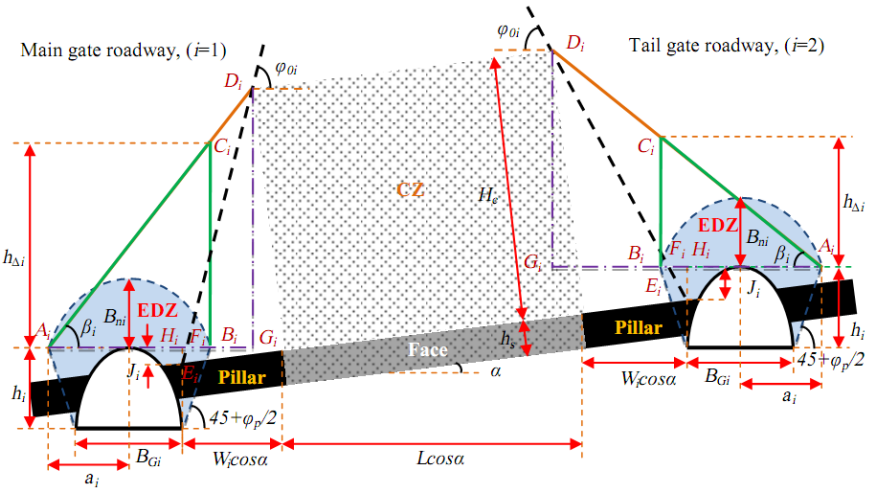

Figure 3. 2D form of GCM for calculating the working effect on the gate roadways considering advance longwall mining [8, 9].

The height of triangle $A_iB_iC_i$ depends on the height of CZ. In order to calculate the area of this triangle, the CZ height must be calculated first. Many researchers have investigated the CZ characteristics [9-18]. It should be noted that GCM could consider any relationship to calculate the CZ height; however, due to the arithmetic model presented in 2012 [19], it is suggested to use the non-linear relationship of arithmetic model (Eq. 3). Based on the arithmetic model, the CZ height is a non-linear function of two parameters, namely the coal seam thickness and the expansion factor of broken rock within CZ (d), and it includes the Peng model as well [19].

$$H_C = \frac{h_s(h_s+3d)}{2d} \tag{3}$$

Based on GCM, the height of triangle $A_iB_iC_i$ is determined as:

$$h_{\Delta i} = \left(B_{Gi} + (2h_i \tan(45-\varphi_p/2)\right)\tan\beta_i \tag{4}$$

Moreover, considering GCM, the influence angle of CZ (β) and the caving angle (φ_0) of the main gate and tail gate roadways are calculated by Eqs. (5)-(8), respectively.

$$\beta_1 = \tan^{-1}\left(\frac{\left(\frac{H_c\sin\phi_{01} - J_1\sin(\phi_{01}-\alpha)}{\sin\phi_{01}\sin(\phi_{01}-\alpha)}\right)\sin\phi_{01}}{\left[B_{Gi} + h_i\tan(45-\phi_p/2)\right] + \left(\frac{J_1 + D_1G_1}{\tan\phi_{0i}}\right)}\right) \tag{5}$$

$$\varphi_{01} = \tan^{-1}\left(\frac{H_c}{W_1}\right) + \alpha \tag{6}$$

$$\beta_2 = \tan^{-1}\left(\frac{\left(\frac{H_c\sin\phi_{02} - J_2\sin(\phi_{02}+\alpha)}{\sin\phi_{02}\sin(\phi_{02}+\alpha)}\right)\sin\phi_{02}}{\left[B_{Gi} + h_i\tan(45-\phi_p/2)\right] + \left(\frac{J_1 + D_1G_1}{\tan\phi_{0i}}\right)}\right) \tag{7}$$

$$\varphi_{02} = \left|\tan^{-1}\left(\frac{H_c}{W_2}\right) - \alpha\right| \tag{8}$$

Therefore, the area of triangle $A_iB_iC_i$ and the area of the extended part of EDZ can be calculated as follow:

$$S_{\Delta i} = \left[\frac{B_{Gi} + h_i\tan(45-\varphi_p/2)}{2}\right]h_{\Delta i} \tag{9}$$

$$S_{add,i} = \frac{1}{48}\frac{a_i h_{\Delta i}^{\,2}(12B_{ni} - h_{\Delta i})}{B_{ni}^{\,2}} \tag{10}$$

Also, the area of extended EDZ (total area of EDZ) is determined as:

$$S_{ext,i} = S_{par,i} + S_{add,i} \tag{11}$$

where, the parabolic area of EDZ is calculated using the following equation:

$$S_{par,i} = \frac{2}{3}\left[B_{Gi} + h_i\tan(45-\varphi_p/2)\right]B_{ni} \tag{12}$$

Considering the area of extended EDZ and Eq. (12), height of the extended EDZ ($B_{ni,ext}$) is calculated as:

$$B_{ni,ext} = \frac{3S_{ext,i}}{2\left[B_{Gi} + h_i\tan(45-\varphi_p/2)\right]} \tag{13}$$

Considering B_{ni}=$B_{ni,ext}$ and Eq. (2), the equivalent height of overburden ($H_{E,i}$) is determined from Eq. (14) and the total roof displacement due to the extended EDZ ($u_{i,ext}$) can be calculated by setting H_i=$H_{E,i}$ in Eq. (1).

$$H_{E,i} = \frac{\sigma_{cm}}{0.03}\ln\left(\left(\frac{3S_{ext,i}}{4B_{Gi}\left[B_{Gi} + h_i\tan(45-\phi_p/2)\right]}\right)^{1.67} + 1\right) \tag{14}$$

Eq. (13) shows the height of extended EDZ above a gate roadway at depth of H_i, which is under the face effect. Characteristics of the extended EDZ could be similar to those of EDZ for a gate roadway at depth of $H_{E,i}$ without any face effect on the gate roadway. Therefore, the concept of difference between H_i and $H_{E,i}$ is used for calculating the face influence coefficient (FIC_i) as in Eq. (15). It should be noted that FIC_i is equal to 1 when there is no influence from the longwall face on the gate roadway [8, 9].

$$FIC_i = \frac{H_{E,i}}{H_i} \tag{15}$$

3. 3D form of GCM (3GCM)

In order to calculate the induced stress fields ahead and behind of the face, it have to take into account the deformation fields above the longwall working and the stress-strain behavior of caving zone. Therefore, firstly, the stress-strain behavior of caving zone is investigated.

3.1. Investigation of stress-strain behavior of caving zone

Due to the destruction of working roof in the face behind, the immediate roof layers break down and the characteristics of the broken material will change constantly before the failure. In this situation, the expansion factor and the residual strength of the fractured rock, control the compression conditions of the broken layers and the stress-strain behavior of caving zone. The values of these parameters have an inverse relation together, so that in higher resistance rocks, the expansion factor is smaller and in the weaker rocks, the expansion factor is larger. In this regard, Salamon considered the relation between the expansion factor and the residual strength of fractured rocks and proposed an equation to study the stress-strain behavior [20].

$$\sigma = \frac{E\varepsilon}{1-\frac{\varepsilon}{\varepsilon_m}} \tag{16}$$

where, σ is the vertical stress, ε is the strain due to vertical stress, E is the tangential modulus, and ε_m is the maximum strain at the expanded layers.

The tangential modulus and strain are calculated as [21]:

$$E = \frac{10.39\sigma_c^{1.042}}{(1+d)^{7.7}} \tag{17}$$

$$\varepsilon_m = \frac{d}{1+d} \tag{18}$$

where, σ_c is the uniaxial compressive strength of intact rock.

3.2. Investigation of deformation and settlement condition above the caving zone

As shown in Figure 4, after destruction of the working roof, three zones are formed above it, which are: caving zone, fractured zone, and deformation zone. The size of each zone depends on the overburden characteristics and the layer thicknesses. In the previous sections, the caving zone was introduced. Since the fractured zone is located after the caving zone, its layers are broken down and expanded due to destruction of the lower layer (the layers bend, without falling). The shape of this zone is completely dependent on the overburden characteristics, and it changes from arched to horse saddle [2]. The vertical expansion value of the fractured zone can be calculated as [22]:

$$S_f = \frac{0.4h_s}{c_3h_s + c_4} \tag{19}$$

where, the values for c_3 and c_4 are obtained from Table 1.

After this zone, the deformation zone is located. It is the nearest zone to the ground level and the furthest zone from the longwall working; hence, due to the low influence of mining operation, the layers bend downward without any major and significant cracks so that, they can be considered as a continuous zone [2].

Considering the characteristics of above zones, the ground surface settlement is a function of three factors: 1) the deformation caused by the caved material within the caving zone; 2) the subsidence or bending of the lowest layer which is, without any caving, fractured; and 3) the vertical expansion of fractured zone. As shown in Figure 5, the maximum deformation of the caved material in the interface of caving and fractured zones (upper surface of the caving zone) (S_{gm}) can be calculated by Eq. (20) [10].

$$S_{gm} = S_m + S_f - S_s \tag{20}$$

In Eq. (20) and Figure 5, S_m is the maximum settlement at ground surface, S_s is the bending value at the lowest non-caved layer, X is the distance from the face, S_x is the surface ground settlement at the distance X, H_f is the height of fractured zone, and H_b is the height of deformation zone. S_s can be calculated as:

$$S_s = 0.05h_s^{1.2} \tag{21}$$

Table 1. Coefficients for calculating vertical expansion at the fractured zone [22].

Resistance condition	σ_c *(MPa)*	Coefficients	
		c_3	c_4
Hard and strong	>40	1.2	2
Medium	20-40	1.6	3.6
Soft and weak	<20	3.1	5

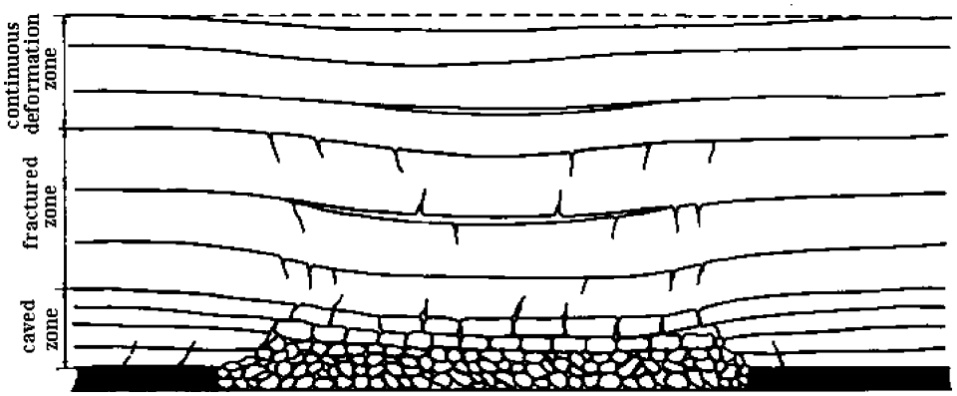

Figure 4. Types of disturbed zones due to mining operations at the longwall working [2].

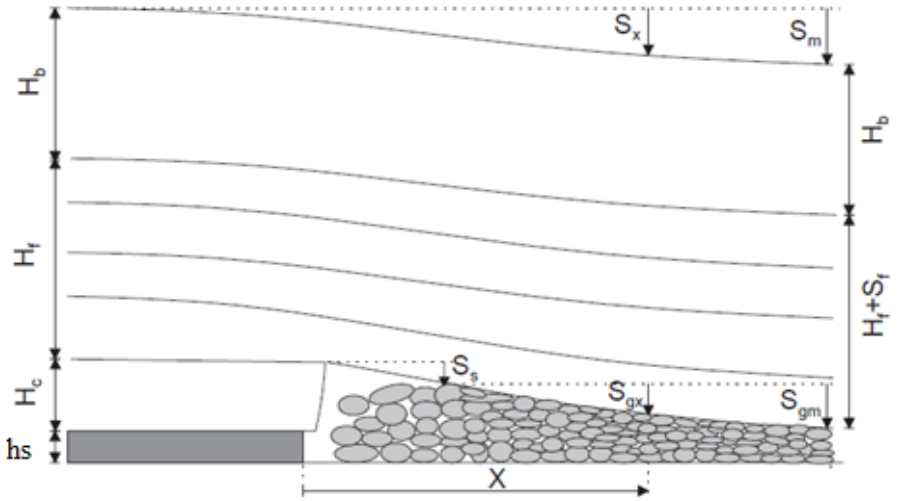

Figure 5. Deformation conditions above the longwall working [10].

Taking into account the geometric conditions of working and caving zone, the strain corresponding to the maximum deformation (S_{gm}) is obtained by the following equation:

$$\varepsilon_{gm} = \frac{S_{gm}}{H_c + h_s} \tag{22}$$

Considering Eq. (3), Eq. (22) is rewritten as follows:

$$\varepsilon_{gm} = \frac{2d\left(S_m + S_f - S_s\right)}{h_s\left(h_s + 5d\right)} \tag{23}$$

Since the strain value in Eq. (16) is equal to ε_{gm}, another relation is obtained for the maximum strain calculation, as:

$$\varepsilon_{gm} = \frac{\sigma}{E + \left(\frac{\sigma}{\varepsilon_m}\right)} \tag{24}$$

In the above equation, the vertical initial stress due to the overburden weight is equal to γH. Considering Eqs. (18) and (24), the maximum vertical strain at the interface of caving and fractured zones is expressed as:

$$\varepsilon_{gm} = \frac{\gamma H d}{Ed + \gamma H\left(1 + d\right)} \tag{25}$$

Eqs. (23) and (25) are equal, and thus taking into account Eqs. (17), (19), and (21), the settlement at ground surface is calculated as:

$$S_m = \frac{1}{2}\left(\frac{\gamma H h_s (h_s+5d)(1+d)^{7.7}}{10.39 d\sigma_c^{1.042}+\gamma H(1+d)^{8.7}}\right) - \frac{0.4h_s}{c_3 h_s + c_4} + 0.05h_s^{1.2} \quad (26)$$

It should be noted that in thin coal seam, the bending and subsidence within the fractured zone does not occur or is very small, and hence, the second and third sentences of Eq. (26) are neglected and the maximum deformation can be calculated from the following equation:

$$S_{gm} = \frac{1}{2}\left(\frac{\gamma H h_s (h_s+5d)(1+d)^{7.7}}{10.39 d\sigma_c^{1.042}+\gamma H(1+d)^{8.7}}\right) \quad (27)$$

3.3. Calculation of induced stress fields at the face behind

To investigate the changes of stress fields in the face behind, deformations at any distance from face (X) have to be determined. In this regard, in 1995, Eq. (28) was proposed to analyze the deformation at the face behind [23].

$$W_x = W_0\left(1-e^{-\frac{X}{2L}}\right) \quad (28)$$

$$L_b = \frac{h}{1-\nu^2}\sqrt{\frac{2\sigma_t}{\gamma H}} \quad (29)$$

where, W_0 is the maximum deformation above the caving zone, L_b is the length of fractured blocks in the upper layer of caving zone, h is the thickness of upper layer of caving zone, σ_t is the tensile strength of upper layer, and ν is the Poisson ratio. Therefore, the deformation at any distance from the face can be calculated by substituting S_{gm} instead W_0 in Eq. (28) as follow:

$$W_X = \frac{1}{2}\left(\frac{\gamma H h_s (h_s+5d)(1+d)^{7.7}}{10.39 d\sigma_c^{1.042}+\gamma H(1+d)^{8.7}}\right)\left(1-e^{-\frac{X}{2L}}\right) \quad (30)$$

Taking into account Eqs. (22) and (30), the strain at any distance from the face can be calculated from Eq. (31).

$$\varepsilon_X = \frac{\frac{1}{2}\left(\frac{\gamma H d h_s (h_s+5d)(1+d)^{7.7}}{10.39 d\sigma_c^{1.042}+\gamma H(1+d)^{8.7}}\right)}{H_c+h_s}\left(1-e^{-\frac{X}{2L}}\right) \quad (31)$$

Now, considering the strain values and Eqs. (16) and (31), the induced stress at face behind (caving region) can be calculated as:

$$\sigma_X = \frac{d\left(\frac{\gamma H d h_s (h_s+5d)(1+d)^{7.7}}{10.39 d\sigma_c^{1.042}+\gamma H(1+d)^{8.7}}\right)}{h_s(h_s+5d)(1+d)^{7.7} - \left(\frac{\gamma H d h_s (h_s+5d)(1+d)^{7.7}}{10.39 d\sigma_c^{1.042}+\gamma H(1+d)^{8.7}}\right)(1+d)^{8.7}}\left(1-e^{-\frac{X}{2L}}\right) \quad (32)$$

3.4. Calculation of induced stress fields at the face ahead

A hypothesis on the vertical induced stress distribution in the face ahead was first proposed by Whittaker and Potts [24]. It was shown that, due to coal extraction, two zones are created in the face ahead, which are namely the high pressure zone (plastic zone) and the low pressure zone (elastic zone) [24]. In 1993, some researchers conducted in-situ monitoring of stress changes surrounding working using a stainless steel borehole platened flat jack (BPF). They showed that the measured stress was almost exactly equal to the original equilibrium pressure distribution as a result of the load being applied symmetrically in three dimensions, which confirmed the reliability of the 'stress balance' method (Figure 6).

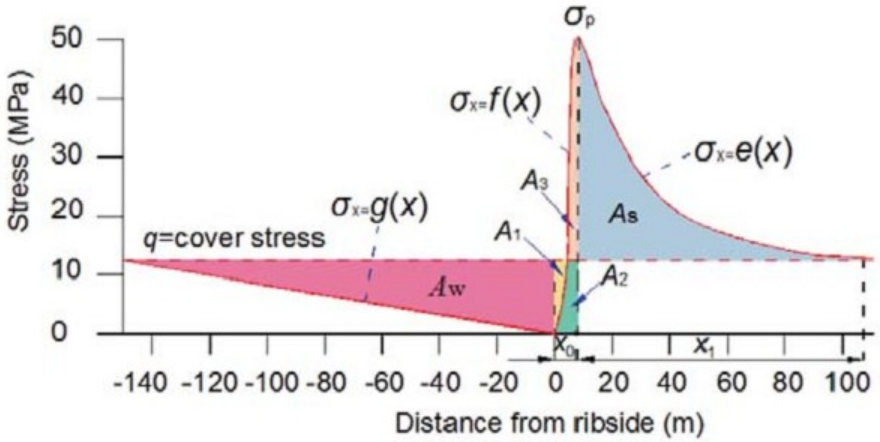

Figure 6. Stress distribution at ahead and behind of the of longwall face [26].

According to the 'stress balance' and referring to Figure 6:

$$A_W + A_1 = A_3 + A_S \quad (33)$$

By adding A_2 to the two sides of the above equation, Eq. (34) is obtained [25].

$$A_W + (A_1 + A_2) = (A_2 + A_3) + A_S \Rightarrow A_W + \gamma H x_b = +A_b + A_S \quad (34)$$

Now, considering Figure 6, the integral form of Eq. (34) can be expressed as:

$$\int_0^{x_a} g(x)dx + \gamma H x_0 = \int_0^{x_0} f(x)dx + \left(\int_{x_0}^{x_b} e(x)dx - q x_1\right) \quad (35)$$

where, x_a is the distance from face at the face behind so that, the vertical induced stress is equal to the vertical initial stress, x_0 is the plastic zone size at the face ahead, x_1 is the elastic zone size at the face ahead, x_b is equal to sum of x_0 and x_1, $f(x)$ is the stress function within the plastic zone, $g(x)$ is the stress function at the face behind, $e(x)$ is the stress function within the elastic zone, A_1, A_2, A_3, A_W, A_S are the areas of under stress curve, and A_b is equal to sum of A_2 and A_3.

According to Eq. (35), with definiteness of each side of the equation, the other side of equation is easily obtained. In 1994 and 2006, mathematical equations were proposed for $f(x)$ and $e(x)$ [27, 28]; however, for $f(x)$, which is representative of induced stress fields within the plastic zone, no attention has been paid to the 3D conditions of primary stress fields. Therefore, in this study, to consider the effects of all the three principal stresses on the induced stress fields within the plastic zone, triaxial unified strength criterion (Eqs. (36) and (37)) was used. The unified strength criterion is capable of reflecting the essential characteristics of rock behavior and is a simple and explicit criterion so that it can consider all stress components and material properties, and moreover, it is easy to use in numerical and analytical modeling [29, 30].

$$\frac{1-\sin\phi}{1+\sin\phi}\sigma_1 - \frac{b\sigma_2 + \sigma_3}{1+b} = \frac{2c\cos\phi}{1+\sin\phi}$$

if (36)

$$\sigma_2 \le \frac{\sigma_1 + \sigma_3}{2} + \frac{\sigma_1 - \sigma_3}{2}\sin\phi$$

$$\frac{1-\sin\phi}{(1+b)(1+\sin\phi)}(\sigma_1 + b\sigma_2) - \sigma_3 = \frac{2c\cos\phi}{1+\sin\phi}$$

if (37)

$$\sigma_2 \ge \frac{\sigma_1 + \sigma_3}{2} + \frac{\sigma_1 - \sigma_3}{2}\sin\phi$$

In Eqs. (36) and (37), σ_1, σ_2, and σ_3 are the major, intermediate, and minor principal stresses, respectively, c is the cohesion of material, φ is the friction angle of material, and b is a constant that reflects the influence of intermediate principal stress and is determined by material mechanical tests such as the true triaxial test. Moreover, it can be calculated by Eq. (38) [29, 30].

$$b = \frac{(\sigma_c + \sigma_t)\tau_0 - \sigma_t\sigma_c}{(\sigma_t - \tau_0)\sigma_c} \quad (38)$$

where, τ is the shear strength.

The parameter b varies from 0 to 1 ($0 \le b \le 1$). In $b = 0$, the unified strength criterion is converted to the Mohr-Coulomb failure criterion, and in $b = 1$, it is converted to Generalized Twin Shear Stress yield. For $0 < b < 1$, the unified strength criterion forms a full spectrum of new criteria [29, 30].

Therefore, considering Eq. (35) and the previous studies and also the unified strength failure criterion, Eqs. (39) and (40) are suggested for $f(x)$ and $e(x)$, respectively. In Eqs. (39) and (40), G_1 to G_4 are obtained from Eqs. (41) to (44), and x_0 is calculated by Eq. (45).

$$f(x) = \left(\frac{1}{\lambda}(F_c x_0 \sin\alpha) + G_1\right)\exp(G_2 + G_3 X + G_4) \quad (39)$$

$$e(x) = K'\gamma H e^{\frac{2\xi}{h_s\lambda}(x_0 - X)} \quad (40)$$

$$G_1 = \frac{2\left(\frac{2(1+b)c_0\cos\varphi_0}{2+b+b\sin\varphi_0}\frac{1}{\cos\varphi_0}\right) - h_s F_c \sin\alpha}{2\tan\left(\sin^{-1}\frac{(2+2b)\sin\varphi_0}{2+b+b\sin\varphi_0}\right)} \quad (41)$$

$$G_2 = \frac{h_s\lambda F_c\cos\alpha - 2\tan\left(\sin^{-1}\frac{(2+2b)\sin\varphi_0}{2+b+b\sin\varphi_0}\right)}{2\lambda} \quad (42)$$

$$G_3 = \frac{2\tan\left(\sin^{-1}\frac{(2+2b)\sin\varphi_0}{2+b+b\sin\varphi_0}\right)}{h_s\lambda} \tag{43}$$

$$G_4 = \frac{h_s}{2}\left(\frac{2\tan^2\left(\sin^{-1}\frac{(2+2b)\sin\varphi_0}{2+b+b\sin\varphi_0}\right)}{h_s\lambda} - F_c\cos\alpha\right) \tag{44}$$

$$x_0 = \chi\frac{h_s\lambda}{2\tan^2\left(\sin^{-1}\frac{(2+2b)\sin\varphi_0}{2+b+b\sin\varphi_0}\right)}\ln\left(\frac{\lambda\left(K'\gamma H\cos\alpha\tan\left(\sin^{-1}\frac{(2+2b)\sin\varphi_0}{2+b+b\sin\varphi_0}\right)+2c_0-h_sF_c\sin\alpha\right)}{\lambda\left(2c_0-h_sF_c\sin\alpha\right)+2P_x\tan\left(\sin^{-1}\frac{(2+2b)\sin\varphi_0}{2+b+b\sin\varphi_0}\right)}\right) \tag{45}$$

In the above-mentioned equations, λ is the stress ratio, F_c is the stress due to body force of coal seam, c_0 is the cohesion between coal seam and working floor, φ_0 is the internal friction angle between the coal seam and the working floor, ξ is the friction coefficient between the layers and K' stress concentration coefficient that is calculated as:

$$K' = \frac{2.729\left(\eta\sigma_{c,coal}\right)^{0.729}}{\gamma H} \tag{46}$$

where, η is the rheology coefficient of coal seam and $\sigma_{c,coal}$ uniaxial compressive strength of coal [27].

According to Eqs. 39-45, the horizontal stress effect is considered by applying the parameter of stress ratio (λ). The horizontal stress has the role of confining stresses surrounding longwall working. In face ahead, because coal seam has not been extracted yet, the confining stress is completely active and plays an important role in the trend of vertical induced stress, and thus Eqs. (39) and (40) show that the sizes of elastic and plastic zones are functions of the stress ratio so that in the larger values of stress ratio, induced stresses converge to initial stress at far distances. However, due to large dimensions of the extracted space behind the face, the confining stress effect is greatly reduced; therefore, the rock layers break down faster due to the vertical initial stress.

3.5. Calculation of induced stress fields in the lateral pillar

According to the R-R section in Figure 1 and the recent studies, the stress trend from the longwall working center towards the lateral pillars are similar to the changes of induced stresses ahead and behind of the longwall face, and the only difference is that the caving region is clinging to the pillar [2, 28]. Therefore, applying the changes in Eqs. (39) and (40), these equations can be used to calculate the induced stress fields in half the working length (half the extraction panel) and within pillars. These changes are as follow:

1) For reinforced pillars (e.g. rock bolts) within gate roadways, the force applied from the support system (P_x) has to be considered in Eq. (39);

2) In inclined workings, the dip effect coefficient of working (K_α) has to be considered in the calculation of the stress concentration coefficient.

Using GCM, the dip effect coefficient of working can be calculated from Eq. (47). Therefore, the stress equation within the plastic zone is similar to Eq. (48), and the stress concentration coefficients for the pillar between the working and main gate roadway and for the pillar between the working and tail gate roadway are calculated by Eqs. (49) and (50), respectively.

$$K_\alpha = \frac{\left(\frac{H_c\sin\varphi_{01}-J_1\sin(\varphi_{01}-\alpha)}{\sin\varphi_{01}\sin(\varphi_{01}-\alpha)}\right)\sin\varphi_{01}}{\left(\frac{H_c\sin\varphi_{02}-J_2\sin(\varphi_{02}+\alpha)}{\sin\varphi_{02}\sin(\varphi_{02}+\alpha)}\right)\sin\varphi_{02}} \tag{47}$$

$$f(x) = \left(\frac{1}{\lambda}\left(P_x+F_cx_0\sin\alpha\right)+G_1\right)\exp\left(G_2+G_3X+G_4\right) \tag{48}$$

$$K' = \frac{2.729K_\alpha\left(\eta\sigma_{c,coal}\right)^{0.729}}{\gamma H} \tag{49}$$

$$K' = \frac{2.729\left(\eta\sigma_{c,coal}\right)^{0.729}}{\gamma HK_\alpha} \tag{50}$$

4. 3GCM application

Two longwall mines were considered in order to investigate the applicability of 3GCM. For this purpose, firstly, the results of 3GCM were compared to a Chinese coal mine actual data to validate the capability of 3GCM and then, the

induced stress in Parvade-2 coal mine in Iran was predicted.

4.1. Validation of 3GCM

In order to validate the performance of 3GCM in calculating the induced stress fields, one of the longwall workings of a Chinese coal mine was considered. The longwall working characteristics are given in Table 2 [31]. In this working, the caving distance from face is 8.8 m, hence, the modeling of induced stresses was carried out at x = 8.8 m. Moreover, the induced stress in the face ahead at x = -40 m and in the face behind at x = 80 m is equal to the initial vertical stress. The maximum vertical induced stress in the face ahead is about 8 Mpa, and the plastic zone size is about 1.1 m.

In Figure 7, using 3GCM, the changes of vertical induced stress in ahead and behind of the face are shown. As it can be seen, the general trend of graph is quite similar to the stress graph for the c-c section in Figure 1, and therefore, it has a reasonable and logical process. Moreover, the vertical induced stresses in ahead and behind of the face is equal to the vertical induced stress at approximately x = -40 m and x = -80 m (in Figure 7, the distance with a negative sign representing the face ahead, and with a positive sign is related to the face behind). Also, the maximum induced stress in the face ahead is 7.8 MPa, which occurs at x = -1.1 m from the face. The trend in the graph showed to be logical, and there is an appropriate agreement between the results obtained by 3GCM and the results presented in Ref. [31].

Table 2. The input data for validation [31].

Parameter	Value	Parameter	Value
γH (MPa)	3.72	$\sigma_{c,coal}$ (MPa)	8.45
λ	0.45	d	0.3
α (deg)	8	ν	0.23
φ_0 (deg)	32	γ_0 (MPa)	0.014
c_0 (MPa)	2	ξ	0.01
h_s (m)	2.2	η	0.5
σ_t (MPa)	1.6	b	0
σ_c (MPa)	11.3	-	-

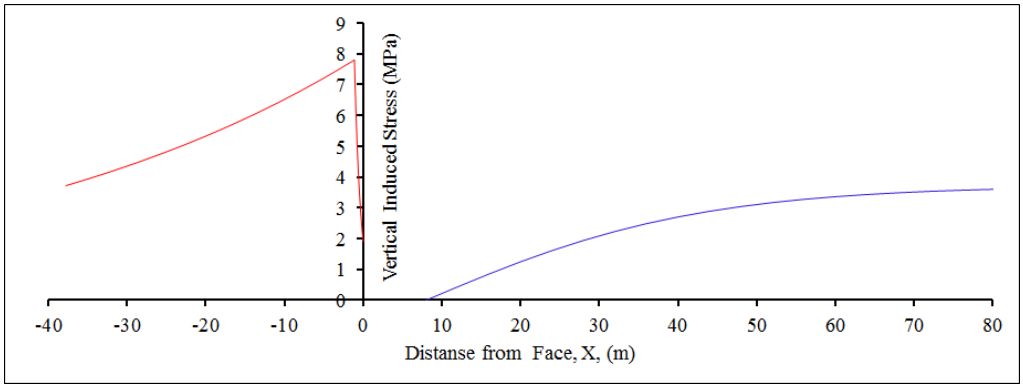

Figure 7. Changes of vertical induced stress in the ahead and behind of face by 3GCM.

4.2. Prediction induced stresses in a Parvade-2 coal mine of Tabas

The Parvade-2 coal mine, with an area of about 40 km^2 and a total reserve of about 5 million tones, is one of five coal areas of Tabas consisting of three coal seams B_1, B_2, and C_1, in which C_1 and B_2 have a high extraction possibility. Coal seam B_2 is extracted by advancing and retreating longwall mining. Thickness of B_2, including 37% of mine reserve (1500000 ton), varies from 0.4 m to 1.75 m. Hangingwall of B_2 consists of siltstone, sandy siltstone, sandstone, and the footwall consists of argillite and sandstone. The length of selected working is 88 m and to protect the main gate roadway and tail gate roadway, pillars with width of 15 m and 3 m are considered. The depths of main and tail gate roadways are 120 m and 64 m, respectively. Moreover, the width and height of both gate roadways are 3.60 and 2.60 m, respectively [8, 9].

Due to high convergence in the supported main gate roadway, displacements of each gate roadway are measured using instrumentation and monitoring operation. Results show that the face effect on the main gate roadway is very high and the maximum convergence at the roof is about 45 cm, whereas for the tail gate roadway, due to the low face effect, the maximum roof displacement

is about 9.5 cm. A comparison of the main gate roadway before and after convergence is shown in Figure 8 [8, 9].

According to the 2D GCM modeling in the previous studies to determine the convergence of tail gate and main gate roadways, it was detected that for the main gate roadway, the face influence coefficient of 4.76 is obtained. Moreover, the roof displacement at q_1 = 60 kPa, considering the face effect, is 42.78 cm. Also, at the tail gate roadway, the face influence coefficient is equal to 2.93 and the roof displacement at q_2 = 60 kPa, is 8.98 cm [8, 9]. The other input data for modeling the 3D induced stress fields in the Parvade-2 coal mine using 3GCM (in the ahead and behind of face and pillars) is mentioned in Table 3.

Figure 8. Comparison of the main gate roadway situations before and after convergence, Parvade-2 coal mine [9].

Table 3. Characteristics of the longwall working, Parvade-2 coal mine.

Parameter	Value	Parameter	Value
γH (MPa)	2.3	d	0.12
λ	1.1	ν	0.24
α (deg)	28	γ_0 (MPa)	0.014
φ_0 (deg)	18	ξ	0.01
c_0 (MPa)	0.95	η	0.5
h_s (m)	1.8	b	0
σ_t (MPa)	1.1	J_1	0
σ_c (MPa)	30	J_2	0
P_x (MPa)	0	-	-

Figure 9 shows the changes of vertical induced stress in the ahead and behind of face. Since the length of working support is about 5 m, the distance of the caving zone from the face is 5 m, and consequently, the study of induced stress fields starts from x = 5 m. By increasing the distance from face, the induced stresses in the face behind is increased non-linearly so that at about x = 70 m, the difference between the vertical induced stress and the vertical initial stress is negligible. Moreover, at x = 120 m, the vertical induced stresses is equal to the vertical initial stress completely and the maximum settlement at the ground surface occurs. In the face ahead, the plastic zone size is equal to 3.2 m, and the vertical induced stress would be reduced by increasing the distance from the plastic zone (induced stresses within the elastic zone) so that at x=-110 m, it is equal to the vertical initial stress.

Figures 10 and 11 present the vertical induced stress changes in the lateral pillars. There are two important issues to be noted: 1) The main and tail gate roadways are protected by pillars of 15 m and 3 m width, respectively; however, in Figures 10 and 11, to study the changes of induced stress in dip direction of coal seam, the width of pillar is not limited to these values. 2) According to the R-R section in Figure 1, at the working center (half

of the working length), the vertical induced stress is almost equal to the vertical initial stress, and thus the changes of induced stress behind the pillar has been investigated for half of the working length.

As shown in Figure 10, for the pillar of main gate roadway, at x = 50 m and x = -150 m, the vertical induced stress is equal to the vertical initial stress (σ_0 = 2.76 MPa). Moreover, the maximum vertical induced stress within the pillar is 11.6 Mpa, which occurs at x = -4 m. Also, according to Figure 11, for pillar of tail gate roadway, the vertical induced stress and the vertical initial stress are equal together at x = 50 m and x = -110 m (σ_0 = 1.49 MPa). Also, the maximum vertical induced stress within the pillar is 4.02 Mpa, which occurs at x = -1.7 m.

It should be noted that, in Figures 10 and 11, the changes of induced stresses along the working length and surrounding pillars were investigated. In these figures, the induced stress fields within the pillars have been obtained only based on the effect of roof caving within the working, while GCM (Figure 3) shows that the pillar width is a function of the EDZ characteristics as well. Therefore, to design the pillar width, the interaction of secondary stresses between the longwall working and the gate roadway must be considered.

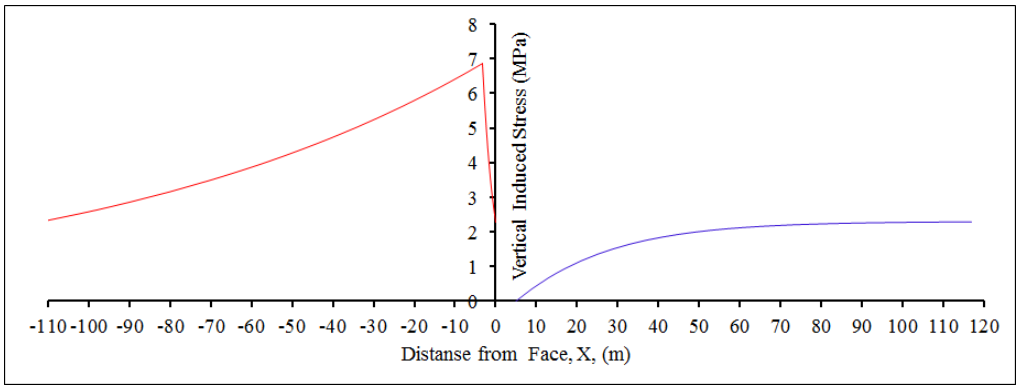

Figure 9. Changes of vertical induced stress at the ahead and behind of face, Parvade-2 coal mine.

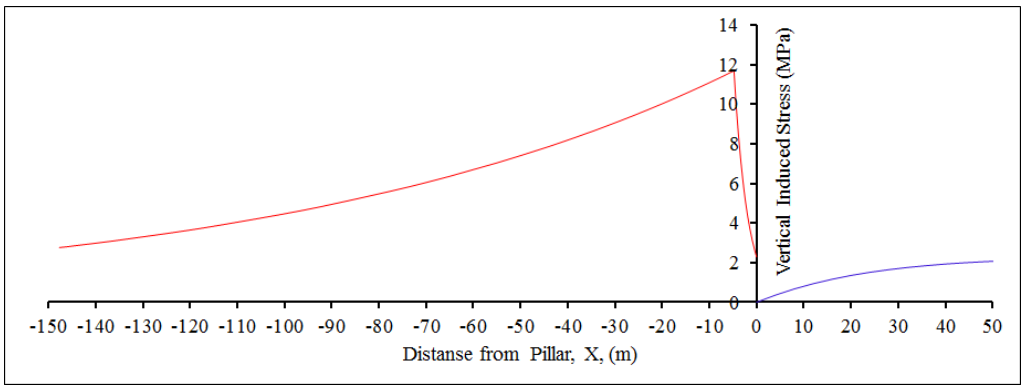

Figure 10. Changes of vertical induced stress surrounding pillar of main gate roadway, Parvade-2 coal mine.

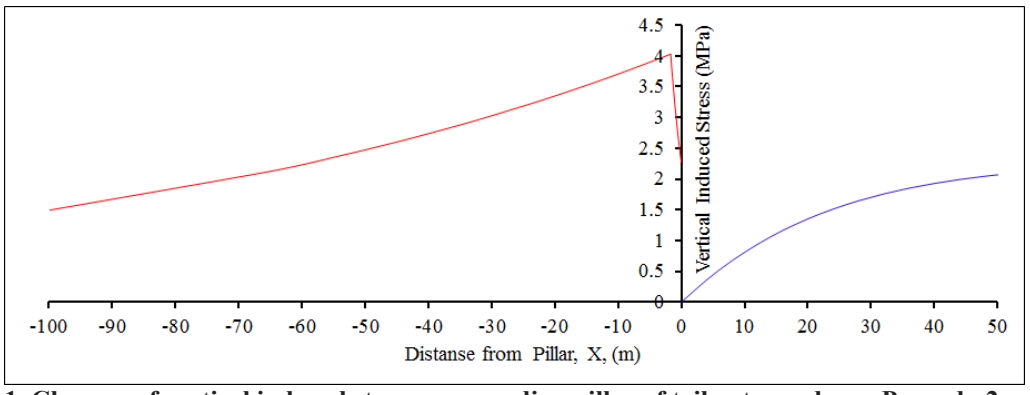

Figure 11. Changes of vertical induced stress surrounding pillar of tail gate roadway, Parvade-2 coal mine.

5. Conclusions

In this paper, a 3D geometrical computing model (3GCM) has been developed to calculate the induced stress fields within the lateral pillars and surrounding longwall face, and the following results were obtained.

1- Based on the validation results, 3GCM is a highly flexible computing model for modeling the vertical induced stress fields surrounding the longwall working.

2- The structure of 3GCM is independent from the cross-section of gate roadways and working length. Therefore, it can be used for mechanized and non-mechanized longwall workings with any cross-section form of gate roadways, and even applicable to the retreating longwall method and the design of chain pillars.

3- 3GCM was used to calculate the vertical induced stresses in one of the longwall workings of the Parvade-2 coal mine. The results obtained show that the maximum induced stress in the face ahead is 6.9 MPa, and the size of the high-pressure zone (plastic zone) is 3.2 m.

4- The analysis of vertical induced stress fields on the lateral pillars show that the working dip has a great influence on the trend of induced stresses within the pillars so that, in the Parvade-2 coal mine, the maximum induced stress at the pillar of main gate roadway is about 3 times larger than the pillar of tail gate roadway.

References

[1]. Brady, B.H.G. and Brown, E.T. (2005). Rock mechanics for underground mining, 3rd edition, Springer. 628 P.

[2]. Peng, S.S. (2006). Longwall mining, 2nd edition, Society for Mining, Metallurgy and Exploration, Inc. (SME). 621 P.

[3]. Peng, S.S. (2008). Coal mine ground control, 3rd edition, John Wiley & Sons, Inc., New York. 750 P.

[4]. Janas, P., Snuparek, R. and Krejsa, M. (2009). Probabilistic approach to designing anchor support in mine workings in Ostrava-Karvina coal district. Tunelling. 4: 37-43.

[5]. Yuehua, D., Jianxin, T., Xiangke, Z., Yong, F. and Zhangyin, D. (2010). Analysis and application in controlling surrounding rock of support reinforced roadway in gob-side entry with fully mechanized mining. Mining Science and Technology. 20: 839-845.

[6]. Snuparek, R. and Konecny, P. (2010). Stability of roadways in coalmines alias rock mechanics in practice. Journal of Rock Mechanics and Geotechnical Engineering. 2 (3): 281-288.

[7]. Jiao, Y.T., Song, L., Wang, X.Z. and Adoko, A.C. (2013). Improvement of the U-shaped steel sets for supporting the roadways in loose thick coal seam. International Journal of Rock Mechanics and Mining Sciences. 60: 19-25.

[8]. Mohammadi, H., Ebrahimi Farsangi, M.A., Jalalifar, H. and Darbani, H. (2016). Development of GCM for Determining the Longwall Working Effect Based on the Different Models of Caving Zone, 3rd National Iranian Coal Congress, Iran.

[9]. Mohammadi, H., Ebrahimi Farsangi, M.A., Jalalifar, H. and Ahmadi, A.R. (2016). A Geometric Computational Model for Calculation of Longwall Face Effect on Gate Roadways. Rock Mechanics and Rock Engineering. 49 (1): 303-314.

[10]. Yavuz, H. (2004). An estimation method for cover pressure re-establishment distance and pressure distribution in the goaf of longwall coal mines. International Journal of Rock Mechanics and Mining Sciences. 41: 193-205.

[11]. Lawrence, W. (2009). A method for the design of longwall gate road roof support. International Journal of Rock Mechanics and Mining Sciences. 46: 789-795.

[12]. Chuen, L.T. (1979). Practice and knowledge of coal mining under water bodies, 10th World Mining Congress, Istanbul, Turkey. pp. 1-15.

[13]. Singh, M.M. and Kendorski, F.S. (1981). Strata disturbance prediction for mining beneath surface water and waste impoundments, Proc. 1st Conference on Ground Control in Mining. pp. 76-89.

[14]. Peng, S. and Chiang, H. (1984). Longwall mining. John Wiley & Sons, Inc., New York. 708 P.

[15]. Fawcett, R.J., Hibberd, S. and Singh, R.N. (1986). Analytic calculations of hydraulic conductivities above longwall coal face. Intertional Journal of Mine Water. 5 (1): 45-60.

[16]. Zhou, Y. (1991). Evaluating the impact of multi-seam mining on recoverable coal reserves in an adjacent seam. Virginia Division of Mineral Resources, Commonwealth of Virginia, Department of Mines, Minerals and Energy, Pub Num. 104 P.

[17]. Suchowerska, A.M., Merifield, R.S., Carter, J.P. and Clausen, J. (2012). Prediction of underground cavity roof collapse using the Hoek–Brown failure criterion. Computers and Geotechnics. 44: 98-103.

[18]. Gao, F., Stead, D., Kang, H. and Wu, Y. (2014). Discrete element modelling of deformation and damage of a roadway driven along an unstable goaf-A case study. International Journal of Coal Geology. 127: 100-110.

[19]. Majdi, A., Hassani, F.P. and Yousef Nasiri, M. (2012). Prediction of the height of distressed zone above the mined panel roof in longwall coal mining. International Journal of Coal Geology. 98: 62-72.

[20]. Salamon, M.D.G. (1990). Mechanism of caving in longwall coal mining, Rock Mechanics Contribution and Challenges. Proceedings of the 31st US Symposium on Rock Mechanics, Golden, CO. CRC Press, Boca Raton, FL. pp. 161-168.

[21]. Yavuz, H. (2004). An estimation method for cover pressure re-establishment distance and pressure distribution in the goaf of longwall coal mines. International Journal of Rock Mechanics and Mining Sciences. 41 (2): 193-205.

[22]. Bai, M., Kendorski, F. and Van Roosendaal, D. (1995). Chinese and North American high-extraction underground coal mining strata behavior and water protection experience and guidelines, Proceedings of the 14th International Conference on Ground Control in Mining, Morgantown. pp. 209-217.

[23]. Miao, X.X. and Qian, M.G. (1995). Solid structure and model of voussoir beam of face surrounding rock. Ground Pressure and Strata Control. 3: 3-12.

[24]. Whittaker, B.N. and Potts, E.L. (1974). Appraisal of strata control practice: Discussion on by B.N. Whittaker, and authors' reply. International Journal of Rock Mechanics and Mining Sciences & Geomechanics Abstracts. 11 (11): A225.

[25]. Compoli, A.A., Barton, T.M., Vandyke, F.C. and Gauna, M. (1993). Gob and gate road reaction to longwall mining in bump-prone strata, US Department of the Interior, Bureau of Mines.

[26]. Wilson, A.H. (1983). The stability of underground workings in the soft rocks of the coal measures. International Journal of Mining Engineering. 1 (2): 91-187.

[27]. Chen, Y. and Qian, M. (1994). China's Coal Mining Strata Control. Coal Industry Press, Beijing.

[28]. Xie, G.X., Yang, K. and Liu, Q.M. (2006). Study on distribution laws of stress in inclined coal pillar for fully-mechanized top-coal caving face. Chinese Journal of Rock Mechanics and Engineering. 25 (3): 545-549.

[29]. Yu, M.H. (2004). Unified strength theory and its applications. Berlin Heidelberg, Springer & Verlag. 447 P.

[30]. Yu, M.H., Ma, G.W., Qiang, H.F. and Zhang, Y.Q. (2006). Generalized plasticity. Springer-Verlag Berlin Heidelberg.

[31]. Wang, W., Jiang, T., Wang, Z. and Ren, M. (2017). An analytical model for cover stress re-establishment in the goaf after longwall caving mining. Journal of the Southern African Institute of Mining and Metallurgy. 117 (7): 671-683.

یک مدل هندسی سه‌بعدی برای محاسبه تنش‌های القایی اطراف کارگاه جبهه کار طولانی

حمید محمدی[1*] و حجت دربانی[2]

۱- گروه مهندسی معدن، دانشکده فنی و مهندسی، دانشگاه ولی‌عصر (عج) رفسنجان، ایران
۲- شرکت زغال‌سنگ نگین طبس، ایران

ارسال ۲۰۱۸/۵/۱۶، پذیرش ۲۰۱۸/۶/۲

* نویسنده مسئول مکاتبات: hamid.mohammadi@vru.ac.ir

چکیده:

در هنگام طراحی معدن به روش استخراج جبهه کار طولانی، بایستی یک سری عوامل و معیارهای مختلف را در کنار همدیگر و هم‌زمان مورد بررسی قرار داد. چالش‌هایی همچون تعیین عرض سقف نگهداری شونده، طراحی سیستم نگهداری، تعیین ارتفاع تخریب، تعیین اندازه پایه‌های جانبی یا زنجیری و طراحی سیستم نگهداری بهینه برای گالری‌های اصلی و فرعی از این دسته عوامل هستند که بایستی مورد توجه قرار گیرند. دقیق‌ترین حالت بررسی تنش‌های القایی اطراف کارگاه استخراج روش جبهه کار طولانی، تحلیل سه‌بعدی است؛ بنابراین هدف اصلی این پژوهش، توسعه یک مدل محاسباتی هندسی سه‌بعدی (3GCM) برای محاسبه تنش‌های القایی در امتداد بارگذاری طولی و عرضی پهنه استخراجی است. 3GCM علاوه بر اینکه قابلیت محاسبه تنش‌های القایی در جلو و پشت جبهه کار را دارد، می‌تواند تغییرات تنش‌های القایی در امتداد طولی جبهه کار و داخل پایه‌های جانبی را نیز بررسی کند. مدل محاسباتی پیشنهاد شده برای تعیین تنش‌های القایی قائم، برای یکی از کارگاه‌های جبهه کار طولانی در معدن زغال‌سنگ پروده ۲ طبس در ایران، مورد استفاده قرار گرفت. اعتبار سنجی 3GCM نشان داد که این مدل محاسباتی، کارایی بالایی برای تحلیل تنش‌های القایی داخل کارگاه استخراج و همچنین اطراف آن دارد.

کلمات کلیدی: 3GCM، جبهه کار طولانی، تنش القایی، معدن‌کاری زغال‌سنگ.